Modeling two-phase flow of immiscible fluids in porous media: Buckley-Leverett theory with explicit coupling terms

Sylvain Pasquier, Michel Quintard, and Yohan Davit[*]
Institut de Mécanique des Fluides de Toulouse, Université de Toulouse, CNRS, INPT, UPS, 31013 Toulouse, France

Continuum models that describe two-phase flow of immiscible fluids in porous media often treat momentum exchange between the two phases by simply generalizing the single-phase Darcy law and introducing saturation-dependent permeabilities. Here we study models of creeping flows that include an explicit coupling between both phases via the addition of cross terms in the generalized Darcy law. Using an extension of the Buckley-Leverett theory, we analyze the impact of these cross terms on saturation profiles and pressure drops for different couples of fluids and closure relations of the effective parameters. We show that these cross terms in the macroscale models may significantly impact the flow compared to results obtained with the generalized Darcy laws without cross terms. Analytical solutions, validated against experimental data, suggest that the effect of this coupling on the dynamics of saturation fronts and the steady-state profiles is very sensitive to gravitational effects, the ratio of viscosity between the two phases, and the permeability. Our results indicate that the effects of momentum exchange on two-phase flow may increase with the permeability of the porous medium when the influence of the fluid-fluid interfaces become similar to that of the solid-fluid interfaces.

I. INTRODUCTION

Modeling two-phase flows of immiscible fluids in porous media is important in many scientific and industrial areas, including petroleum engineering and hydrogeology [1,2], chemical engineering, and nuclear safety [3,4]. The classical mathematical descriptions of momentum transport at the continuum scale are simple extensions of Darcy's law for single-phase flow. The most widespread model corresponds to the generalized Darcy law [5], where the relative influence of one phase on the other one is captured by a relative permeability, which is usually treated as a function of the saturations [6]. In most of these representations, the coupling between the two phases is done by simply correcting effective parameters of models initially developed for single-phase flow.

While generalized Darcy law models are currently being used in engineering practice, research of the past several decades has lead to more elaborate models capable of dealing with complex and dynamic pore-scale physics [7–16]. Among these models, there has been recently a renewed interest in those that include an explicit coupling for the description of mass and momentum exchanges between the phases [3,17]. Cross terms that couple the equations for momentum transport of each phase can be obtained theoretically, either by considering the case of the annular viscous two-phase flow in tubes, for which a simple analytical solution analogous to that of Poiseuille can be derived [18,19], or from upscaling techniques such as the method of volume averaging [16] (more details are in Sec. II A) or homogenization theory [7].

How important are these cross terms? We anticipate that this will strongly depend upon the contact area between the two fluid phases, which in turn is controlled by effects such as the capillary action, wettability, or structure of the porous medium. If the area of the fluid-fluid interface is comparable to the area of fluid-solid interfaces, the coupling terms may be important, whereas if the area of the

fluid-solid interface is much larger than that of the fluid-fluid interface, exchanges may be minimal. The hypothesis that we explore in this paper is that the size of the pores can control the influence of the fluid-fluid and fluid-solid interfaces and therefore exchanges between the two phases. In particular, our idea is that there is a positive correlation between the size of the pores and the effects of the cross terms on momentum transport. This hypothesis is based on a variety of results from the literature that we detail below.

On the one hand, studies such as [20] show that coupling effects are relatively small for water (wetting) and mercury (nonwetting) flowing through packed sand (permeability of about 34×10^{-12} m^2). Zarcone and Lenormand hypothesize that the wetting and nonwetting phases flow through different pore networks, most likely because of capillarity, and therefore minimize the interfacial area between the two fluids. The consequence is that solid-fluid interactions dominate over fluid-fluid interactions. While this is a controversial hypothesis (see, e.g., [18,19,21–23]), there is also circumstantial evidence that coupling effects are small in low-permeability media. For instance, these terms are always neglected in reservoir modeling of water-oil flow through rocks with relatively low permeabilities; typically, permeabilities of the rocks are about 10^{-12} m^2 or less in petroleum engineering.

On the other hand, studies such as [12,18,24,25] indicate that a strong friction between the two phases can occur when the interface area and the permeability are large. Such a strong interaction between phases has also been observed in many chemical engineering or nuclear engineering applications involving regular packed beds or structured packings with large permeabilities (permeabilities of about $10^{-8}-10^{-6}$ m^2). For instance, models of co- and countercurrent flows in trickle beds or structured packings often consist of conservations laws corrected with additional *friction terms* [26] describing phase interactions. This is also the case for boiling-water–steam flows in nuclear debris beds, for which various heuristic models have been developed [27–30]. Experiments for such systems show that many observations *cannot be reproduced* by the classical models without cross terms [3,17,29].

In this paper our goal is to analyze the relative importance of coupling terms in continuum-scale models of two-phase flows in porous media. To do so, we first develop a generic model for two-phase flow of immiscible fluids in porous media with an explicit exchange of momentum between both phases (Sec. II A). We then use the Buckley-Leverett theory (Sec. II B), which is extended to account for the cross terms, to calculate the saturation profiles and their dynamics in a one-dimensional setting (Sec. III). Considering simulations and experimental data from the literature on imbibition (Sec. III) and drainage (Sec. III) for water-air and water-oil interactions, we evaluate the relative influence of the cross terms and their physical relevance depending on the system considered.

II. METHODS

Here we first present a continuum model to describe two-phase flow of immiscible fluids in porous media. We then go on to provide a brief description of the Buckley-Leverett theory (Sec. II B), the configurations studied (Sec. II C), and a list of the different closure relations used (Sec. II D).

A. Models and assumptions

1. Model with cross terms

Continuum models for the creeping flow of two immiscible fluids, phases i and j, involving cross terms for momentum exchanges were initially postulated by Raats in [31] and Baveye and Sposito in [32], often following arguments based on the concepts of irreversible thermodynamics [12,33,34]. Using the volume-averaging theory, Whitaker in [16] derived a model with closure problems for the effective parameters. In this work we will use these expressions from volume averaging as a basis to construct our model. Similar coupled laws were also derived by Auriault in [7] using the method of homogenization and by Marle in [34] using concepts of irreversible thermodynamics.

The mass conservation equation for phases i and j reads

$$\varepsilon \frac{\partial}{\partial t}\begin{pmatrix} S_i \\ S_j \end{pmatrix} + \nabla \cdot \begin{pmatrix} \mathbf{U}_i \\ \mathbf{U}_j \end{pmatrix} = \begin{pmatrix} 0 \\ 0 \end{pmatrix}, \tag{1}$$

with $\mathbf{U}_i$ and $\mathbf{U}_j$ the superficial velocities and ε the porosity of the porous medium. For simplicity, we do not take into account residual saturations, which could be easily treated by changing the saturation variables to the reduced saturations $S_i^\star = \frac{S_i - S_i^{\min}}{S_i^{\max} - S_i^{\min}}$ and $S_j^\star = \frac{S_j - S_j^{\min}}{S_j^{\max} - S_j^{\min}}$.

The momentum transport equations read [16]

$$\mathbf{U}_i = -\frac{\mathbf{K}_{ii}}{\mu_i} \cdot (\nabla P_i - \rho_i \mathbf{g}) + \mathbf{K}_{ij} \cdot \mathbf{U}_j, \tag{2a}$$

$$\mathbf{U}_j = -\frac{\mathbf{K}_{jj}}{\mu_j} \cdot (\nabla P_j - \rho_j \mathbf{g}) + \mathbf{K}_{ji} \cdot \mathbf{U}_i, \tag{2b}$$

where ∇P_i and ∇P_j are the pressure gradients, ρ_i (ρ_j) and μ_i (μ_j) are the density and viscosity of phase i (j), and $\mathbf{g}$ is the gravitational acceleration. In addition, $\mathbf{K}_{ii}$ and $\mathbf{K}_{jj}$ are second-order permeability tensors and $\mathbf{K}_{ij}$ and $\mathbf{K}_{ji}$ are second-order viscous coupling tensors. Equations (2a) and (2b) are the equations that differ from the generalized Darcy law in that we have cross terms $\mathbf{K}_{ij} \cdot \mathbf{U}_j$ and $\mathbf{K}_{ji} \cdot \mathbf{U}_i$ describing momentum exchange between both phases. Lasseux *et al.* showed that this model can be further extended to account for inertial effects by including additional drag terms [35], but we limit our analysis to creeping flow in this paper. In fact, in such cases, the velocity-dependent terms are not compatible with the Buckley-Leverett theory.

The derivation of these models requires several important assumptions. One of these is that the interface between the immiscible fluids remains locally quasistatic, i.e., that the flow at the pore-scale relaxes quickly compared to characteristic time scales of the macroscale process. Another important assumption is that the capillary and Bond numbers, which respectively compare the viscous and gravity effects to surface tension, are much smaller than unity. Alternative models have been proposed to account for dynamic effects (see, for example, [36,37] for the use of pseudofunctions, [11,13,14] for other forms of laws accounting for dynamic effects induced by heterogeneities, multizones, or [10] for the use of the theory of irreversible thermodynamics). However, it is probable that less restrictive assumptions in the upscaling may still yield equations similar to Eqs. (2a) and (2b) for momentum transport, with the same effective parameters but capturing additional physical effects. Further, the expression in Eqs. (2) is used, in a variety of different forms, in engineering applications, where it is successful in describing many different systems [38]. We therefore base our model on the system of equations (1), (2a), and (2b), with simplifications that are described in the next section.

2. Simplifications

The objective of this paper is to emphasize the contribution of the additional terms compared to the behavior of the classical model. Many different initial-boundary-value problems could be used as test cases. However, we will limit our investigation to one-dimensional situations commonly encountered in the laboratory experiments that have been used to study flows and measure transport parameters in such systems. Simplifications that correspond to these most common situations are as follows.

(i) Isotropy. For simplicity, we consider that the tensorial permeabilities $\mathbf{K}_{ii}$ and $\mathbf{K}_{jj}$ can be written as

$$\mathbf{K}_{ii} = K_0 k_{r_i} \mathbf{I}, \quad \mathbf{K}_{jj} = K_0 k_{r_j} \mathbf{I}, \tag{3}$$

where $\mathbf{I}$ is the identity tensor, K_0 is the intrinsic permeability of the medium, and k_{r_i} and k_{r_j} are the relative permeabilities of phases i and j, respectively. This form is based on the assumptions that the porous structure is isotropic and that there is no anisotropy generated by the two-phase flow

itself [39]. Similarly, we write

$$\mathbf{K}_{ij} = K_{ij}\mathbf{I}, \quad \mathbf{K}_{ji} = K_{ji}\mathbf{I}.$$

(ii) Dimensions. We limit our analysis to a one-dimensional system.

(iii) Consistency of the relative permeabilities. We assume that

$$k_{r_i}(S_i = 1) = 1, \quad k_{r_j}(S_i = 1) = 0, \tag{4}$$

$$k_{r_i}(S_i = 0) = 0, \quad k_{r_j}(S_i = 0) = 1, \tag{5}$$

$$K_{ji}(S_i = 1) = 0, \quad K_{ij}(S_j = 1) = 0, \tag{6}$$

which are necessary assumptions to obtain Darcy's law in the limit of single-phase flow.

(iv) Local pressure equilibrium. Assuming that capillary effects are negligible at the macroscale, we write $P_i = P_j \equiv P$ and $\frac{\partial P_i}{\partial x} = \frac{\partial P_j}{\partial x} \equiv \frac{\partial P}{\partial x}$. This assumption holds for flows within highly permeable media, where viscous and inertial effects dominate over the capillary pressures. This will be correct for pores much larger than the capillary length. For air-water flow at standard temperature and pressure, an order of magnitude estimation is therefore that the pores are significantly larger than the millimeter, i.e., that the permeability is larger than about $10^{-9}\,\mathrm{m}^2$. This is consistent with the fact that, as discussed in Introduction, the coupling terms are likely to play a more significant role for highly permeable media.

3. Mass balance

With these assumptions, the mass balance equations now read

$$\varepsilon \begin{pmatrix} \frac{\partial S_i}{\partial t} \\ \frac{\partial S_j}{\partial t} \end{pmatrix} + \begin{pmatrix} \frac{\partial U_i}{\partial x} \\ \frac{\partial U_j}{\partial x} \end{pmatrix} = \begin{pmatrix} 0 \\ 0 \end{pmatrix}. \tag{7}$$

4. Momentum balance with cross terms

Momentum balance equations with cross terms can be written as

$$U_i = -\frac{K_{ii}}{\mu_i}\left(\frac{\partial P}{\partial x} - \rho_i g\right) + K_{ij}U_j, \tag{8}$$

$$U_j = -\frac{K_{jj}}{\mu_j}\left(\frac{\partial P}{\partial x} - \rho_j g\right) + K_{ji}U_i, \tag{9}$$

with gravity collinear and oriented with the basis vector $\mathbf{e}_x$ so that $\mathbf{g} \cdot \mathbf{e}_x = g$. An alternative formulation, initially derived by Lasseux *et al.* [40], can be obtained by combining Eqs. (8) and (9),

$$\begin{pmatrix} U_i \\ U_j \end{pmatrix} + \mathcal{K}^\star \begin{pmatrix} \frac{\partial P}{\partial x} - \rho_i g \\ \frac{\partial P}{\partial x} - \rho_j g \end{pmatrix} = 0. \tag{10}$$

The matrix $\mathcal{K}^\star$ is symmetric and reads

$$\mathcal{K}^\star = \begin{pmatrix} \frac{K_{ii}^\star}{\mu_i} & \frac{K_{ij}^\star}{\mu_j} \\ \frac{K_{ji}^\star}{\mu_i} & \frac{K_{jj}^\star}{\mu_j} \end{pmatrix} = \frac{1}{1 - K_{ij}K_{ji}} \begin{pmatrix} \frac{K_{ii}}{\mu_i} & \frac{K_{jj}K_{ij}}{\mu_j} \\ \frac{K_{ii}K_{ji}}{\mu_i} & \frac{K_{jj}}{\mu_j} \end{pmatrix}. \tag{11}$$

5. *Momentum balance without cross terms (generalized Darcy laws)*

Momentum balance equations without cross terms are simply obtained by setting $K_{ij} = 0$ and $K_{ji} = 0$ in the previous model, so we have

$$U_i = -\frac{K_{ii}}{\mu_i}\left(\frac{\partial P}{\partial x} - \rho_i g\right), \tag{12}$$

$$U_j = -\frac{K_{jj}}{\mu_j}\left(\frac{\partial P}{\partial x} - \rho_j g\right). \tag{13}$$

B. Buckley-Leverett theory

With these simplifications, equations can be grouped together into a single nonlinear hyperbolic equation suitable for an analysis based on the Buckley-Leverett theory.

1. *Formulation*

The Buckley-Leverett theory [41] has been widely used in the literature to analyze the structure of two-phase flows through both homogeneous and heterogeneous media [41–46]. It is also used as a reference to validate numerical solvers [47–50] and to evaluate their accuracy in capturing shocks. Here we consider a one-dimensional domain, with the initial condition $S_j = 1$ and phase i injected at constant flow rate $U_i(0,t)$ for $t > 0$. The Buckley-Leverett problem characterizes the propagation of the fluid front in the domain and can be obtained by combining Eqs. (7)–(9). Introducing the total velocity $U = U_i + U_j$, one obtains the velocity of phase i as

$$U_i = \frac{m_i + K_{ij}m_j}{m_i + m_j + K_{ji}m_i + K_{ij}m_j}U + \frac{m_i m_j}{m_i + m_j + K_{ji}m_i + K_{ij}m_j}(\rho_i - \rho_j)g, \tag{14}$$

where $m_i = \frac{K_{ii}}{\mu_i}$ and $m_j = \frac{K_{jj}}{\mu_j}$ are the mobility parameters. This yields

$$\varepsilon\frac{\partial S_i}{\partial t} + \frac{\partial \mathcal{F}_i}{\partial x} = 0, \tag{15a}$$

$$S_i(x,0) = 0 \quad [S_j(x,0) = 1], \tag{15b}$$

$$U_i(0,t) = \mathcal{F}_i[S_i(0,t)] = U, \quad t > 0, \tag{15c}$$

where $\mathcal{F}_i(S_i)$ is the flux function (also called fractional flow in the Buckley-Leverett theory), which reads

$$\mathcal{F}_i(S_i) = U_i = \frac{m_i}{m_i + m_j}U\left(f_1 + \frac{\mu_i}{\mu_j}\mathcal{N}_g k_{r_j}(S_i)f_2\right). \tag{16}$$

Here $\mathcal{N}_g = \frac{K_0(\rho_i - \rho_j)g}{U\mu_i}$ is the gravity number, $k_{r_j}(S_i)$ is the relative permeability for the phase j, and f_1 and f_2 are functions that characterize the impact of the coupling coefficients K_{ij} and K_{ji} in the momentum balance equations,

$$f_1 = \frac{1 + K_{ij}\frac{m_j}{m_i}}{1 + \frac{K_{ji}m_i + K_{ij}m_j}{m_i + m_j}}, \quad f_2 = \frac{1}{1 + \frac{K_{ji}m_i + K_{ij}m_j}{m_i + m_j}}. \tag{17}$$

2. *Unique solution for the conservation law*

Equation (15a) is a scalar one-dimensional conservation law whose solutions might involve discontinuities. Solving this problem is meaningful only in a weak sense, allowing for discontinuous functions to be solutions. Further, obtaining a unique and physically realistic result requires additional
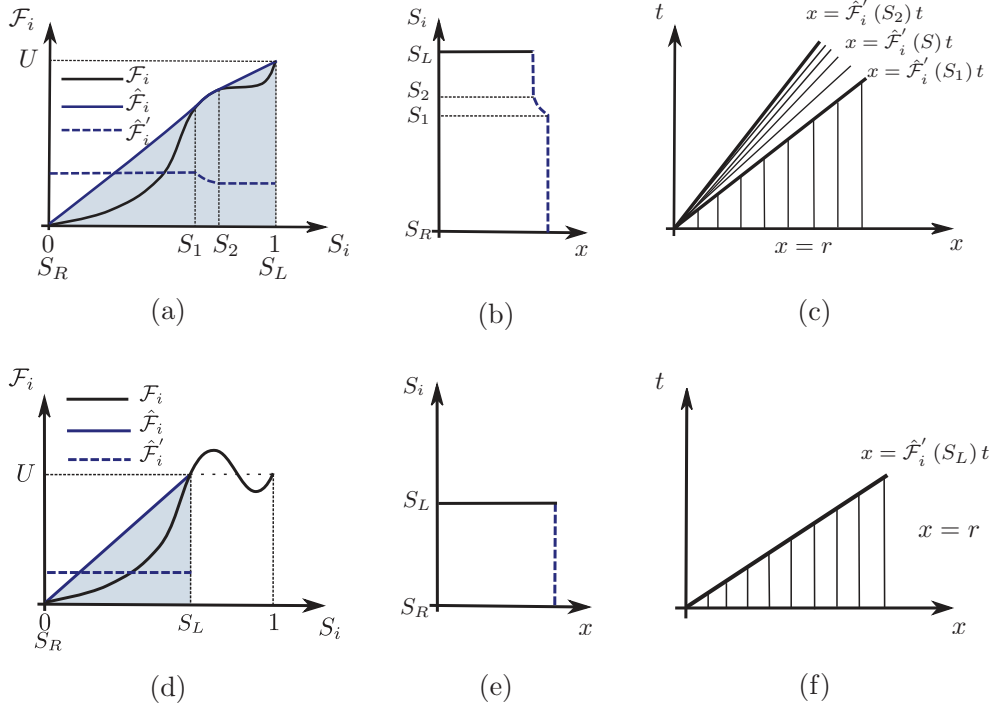
FIG. 1. Construction of the saturation fronts. (a) and (d) Plots of the flux function $\mathcal{F}_i$, the concave hull $\hat{\mathcal{F}}_i$, and its derivative $\hat{\mathcal{F}}_i'$ (see the Appendix). (b) and (e) Corresponding profile of the front S_i along x. (c) and (f) Characteristic curves of the system in the x-t plane. The first (leftmost vertical) line corresponds to $\mathcal{F}_i(S_i) = U$ having a unique solution. The second line corresponds to $\mathcal{F}_i(S_i) = U$ having multiple solutions.

admissibility and entropic conditions. Those are well discussed in the literature [41,46,51–53] and a little summary of methods for constructing solutions is provided in the Appendix.

We present in Fig. 1 the two configurations encountered in this study. In the former case, the inlet condition $\mathcal{F}_i(S_L) = U = U_i(0,t)$ admits $S_L = 1$ as a unique solution (indices L and R for left and right). The solution $S_i(x,t)$ of the Riemann problem admits two shocks between S_L and S_2 and between S_1 and S_R and a rarefaction wave between S_1 and S_2. The unique solution $S_i(x,t)$, shown in Fig. 1(b), reads

$$S_i(x,t) = \begin{cases} S_L & \text{for } x < \hat{\mathcal{F}}_i'(S_1)t \\ S_i(x,t) = (\hat{\mathcal{F}}_i')^{-1}\left(\frac{x}{t}\right) & \text{for } \hat{\mathcal{F}}_i'(S_2) < \frac{x}{t} < \hat{\mathcal{F}}_i'(S_1) \\ S_R & \text{for } x > \hat{\mathcal{F}}_i'(S_2)t, \end{cases} \tag{18}$$

with the concave hull $\hat{\mathcal{F}}_i$ introduced in the Appendix. In the latter case, which is encountered when gravity effects dominate viscous effects, the inlet condition (15c) admits more than one solution. Only one of these solutions has a positive propagation velocity, so the shocks propagate in the same direction as the inlet velocity. Other possible solutions have a shock with a negative propagation velocity, a case that has been previously studied in [53]. The main difference between the case in [53] and the configurations here are the boundary and initial conditions. In the case in [53], a fraction of the medium is initially fully saturated with one phase and the rest is fully saturated with the other phase. Therefore, the values of the saturations are known everywhere, yielding fronts propagating in opposite directions. In our case, the porous medium is initially saturated only with one phase and we impose a velocity U at the inlet, which is the case corresponding to the experimental data that we
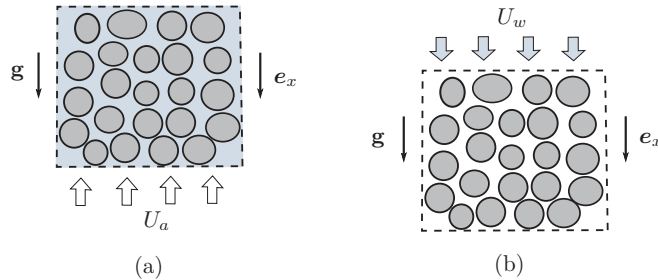
FIG. 2. Illustrations of the two configurations considered: (a) configuration 1, drainage, and (b) configuration 2, imbibition.

use. Given these boundary and initial conditions, we consider that shocks cannot propagate contrary to the inlet velocity and that the only physically realistic solution $S_i(x,t)$ admits one unique shock between S_R and S_L (see the illustration in Fig. 1), which is expressed as

$$S_i(x,t) = S_L \quad \text{for } x < \hat{\mathcal{F}}'_i(S_L)t. \tag{19}$$

As we will see later on, the results obtained with this choice are in very good agreement with experimental data, confirming that this is the correct case for the experimental data considered in this paper.

C. Boundary, initial conditions, and fluids

We consider two boundary-value problems corresponding to two classical configurations encountered in porous media. The first configuration corresponds to the experiments of Chikhi *et al.* in [3], which consists of an air-water system in a particle bed, a configuration known to emphasize the impact of the coupling terms as discussed in [17]. It corresponds to a drainage process, since the nonwetting phase (air) is displacing the wetting phase (water) out of the column. The second configuration describes an imbibition process, where a wetting phase is introduced into a porous medium initially filled with a nonwetting phase. This problem corresponds to the standard use of the Buckley-Leverett theory, for application to oil recovery using water. The two configurations are illustrated in Fig. 2. The fluid properties (density and viscosity) of air, water, and oil are given in Table I.

D. Closures for the effective parameters

We consider two classes of closures for the effective parameters: one obtained from Clavier *et al.* [17] (constructed from experimental data [3]) and one based on the analytical solution of an annular two-phase viscous flow within a capillary tube. These closures are also compared in Sec. III to the one obtained by Rothman in [25], Zarcone and Lenormand in [20], and Kalaydjian in [18].

TABLE I. Fluid properties.

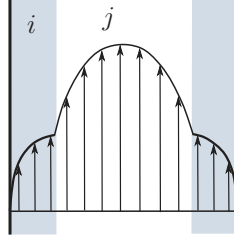|	density ρ (kg/m^3)	viscosity μ (Pa s)
air	1	1.8×10^{-5}
water	10^3	10^{-3}
oil	8×10^2	10^{-1}

FIG. 3. Velocity field in a cross section of a capillary tube illustrating the annular two-phase viscous flow.

1. Configuration 1: Closure from [17], based on experimental data

The first closure relations used in this paper have been recently obtained [17] from the experimental database presented in [3] (CALIDE experiment). The experiments, which focus on water-air flow in a column filled with coarse particles, were part of a large work studying water-steam flows in a debris bed in the context of a severe accident in a nuclear reactor. Air and water are injected from below, with a controlled flow rate, in a vertical column initially saturated with water until a steady state is obtained [sketch in Fig. 2(a)]. The phase saturations were then measured using capacitance probes and the pressure drop was obtained via a differential measure of the pressure. These experiments offer a very valuable database of saturations and pressure drops over a wide range of flow rates. From these data, the authors also derive closures for the effective parameters of the model (Sec. II A). The term K_{ww} of the water phase is assumed to be

$$K_{ww} = K_0 S_w^3, \tag{20a}$$

which also corresponds to a Brooks-Corey correlation. The effective parameters K_{aa} and K_{wa} are then derived from the experimental data as

$$K_{aa} = K_0(1 - S_w)^4, \tag{20b}$$

$$K_{wa} = \beta \frac{\mu_a}{\mu_w} \frac{S_w^2}{(1 - S_w)}, \tag{20c}$$

where β is a factor that weights the amplitude of the cross term and is directly related to the particle size. The term K_{aw} is finally determined using the relation between the nondiagonal coefficients in Eq. (11),

$$K_{aw} = \frac{\mu_w}{\mu_a} \frac{K_{aa} K_{wa}}{K_{ww}} = \beta \frac{(1 - S_w)^3}{S_w}. \tag{20d}$$

2. Configuration 2: Analytical solution of the annular viscous flow

The second closure relations are derived from the analytical solution of an annular two-phase viscous flow (phases i and j) within a capillary tube [54,55] (see Fig. 3 for an illustration)

$$K_{ii} = S_i^2 - 2S_i(1 - S_i) - 2(1 - S_i)^2 \ln(1 - S_i) - 4r_\mu \frac{[S_i + (1 - S_i)\ln(1 - S_i)]^2}{1 - 2r_\mu \ln(1 - S_i)}, \tag{21a}$$

$$K_{jj} = (1 - S_i)^2 - 2r_\mu(1 - S_i)^2 \ln(1 - S_i) - 4r_\mu \frac{(1 - S_i)^2[S_i + (1 - S_i)\ln(1 - S_i)]^2}{S_i^2 - 2S_i(1 - S_i) - 2(1 - S_i)^2 \ln(1 - S_i)}, \tag{21b}$$
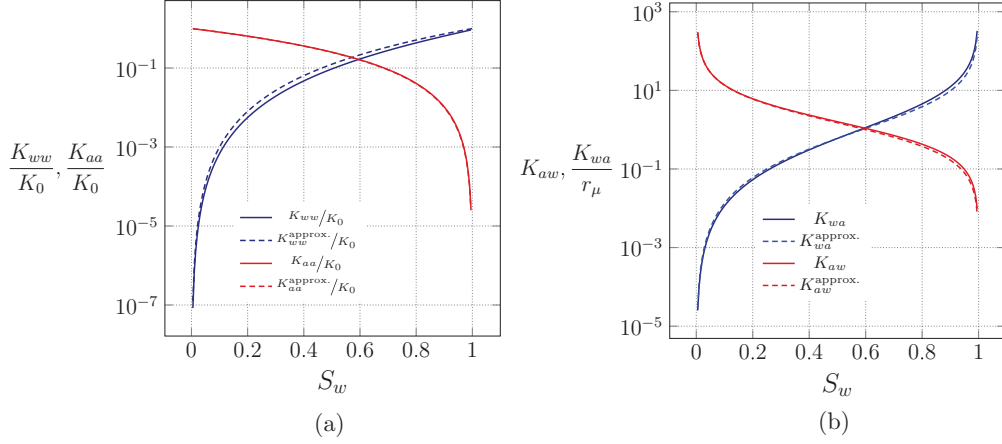
FIG. 4. Comparison of exact [$\frac{K_{ww}}{K_0}$, $\frac{K_{aa}}{K_0}$, K_{wa}, and K_{wa}, from Eqs. (21)] and approximated [$\frac{K_{ww}^{\text{approx}}}{K_0}$, $\frac{K_{aa}^{\text{approx}}}{K_0}$, K_{wa}^{approx}, and K_{wa}^{approx}, from Eqs. (22)] effective properties for the two-phase annular flow, with (a) intrinsic permeabilities and (b) cross terms.

$$K_{ij} = 2r_\mu \frac{S_i + (1 - S_i)\ln(1 - S_i)}{1 - 2r_\mu \ln(1 - S_i)}, \tag{21c}$$

$$K_{ji} = 2(1 - S_i) \frac{S_i + (1 - S_i)\ln(1 - S_i)}{S_i^2 - 2S_i(1 - S_i) - 2(1 - S_i)^2 \ln(1 - S_i)}, \tag{21d}$$

where i is the wetting phase, j is the nonwetting phase, and $r_\mu = \frac{\mu_j}{\mu_i}$ is the viscosity ratio. Clavier [54] suggest simplified expressions in the limit where $r_\mu \ll 1$,

$$K_{ii}^{\text{approx}} = K_0 S_i^3, \quad K_{jj}^{\text{approx}} = K_0 (1 - S_i)^2, \tag{22a}$$

$$K_{ji}^{\text{approx}} = \frac{1 - S_i}{S_i}, \quad K_{ij}^{\text{approx}} = r_\mu \frac{S_i^2}{1 - S_i}. \tag{22b}$$

Here K_{ii}^{approx} and K_{jj}^{approx} correspond to the Brooks-Corey correlations [56] that are used extensively in the literature for two-phase flows in porous media. We see in Fig. 4 that the simplified expressions approximate very well the exact solution for the air-water system when $r_\mu \ll 1$ ($r_\mu = 0.018$).

III. RESULTS

A. Drainage: Water-air flow in a particle bed

We proceed to the computation of the boundary-value problem presented in Fig. 2(a), which is the case of drainage of a water column with air. The analysis is based on the experimental closures presented in Sec. II D 1. Results at steady state are presented for both models and experimental data in Fig. 5. We see that the model with cross terms provides a much more accurate representation of the pressure drop and the liquid saturation for $\frac{1}{\mathcal{N}_g} \lesssim 0.01$. In particular, it captures correctly the variation of the pressure drop that is due to the momentum transfer from the air to the water, when the model without cross terms can only balance $\frac{\partial P}{\partial x}$ with $\rho_w g$ for any flow rate. The dimensionless pressure drop $\frac{1}{\rho_w g} \frac{\partial P}{\partial x}$ is indeed computed at steady state from Eq. (8) as

$$\frac{1}{\rho_w g} \frac{\partial P}{\partial x} = 1 + \frac{\mu_w U_a K_{wa} K_{ww}^{-1}}{\rho_w g}. \tag{23}$$
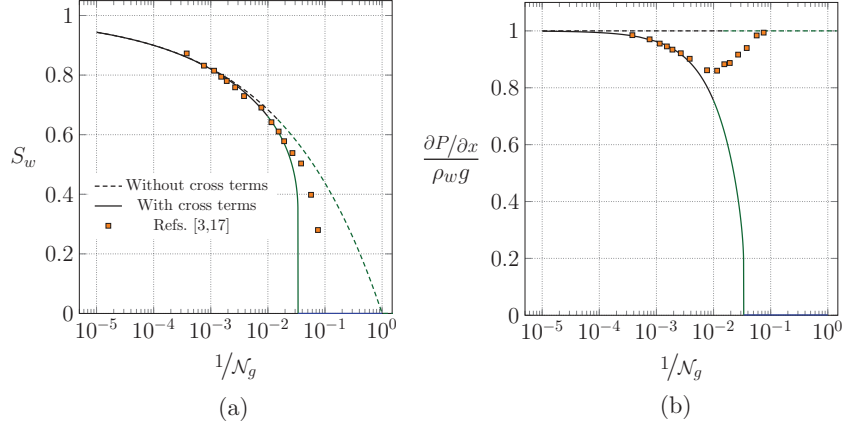
FIG. 5. Comparison of steady-state profiles with (solid lines) and without (dashed lines) cross terms to experimental data from [3,17] with (a) water saturation and (b) the dimensionless pressure gradient as a function of $\frac{1}{\mathcal{N}_g}$. The colors distinguish different regimes of $\mathcal{N}_g$, with a shock (black), a rarefaction wave (blue), or both (green) (see also Fig. 6).

Consistent with the experiment of Tutu *et al.* in [29], these results confirm that the generalized Darcy law fails to recover the flow properties for such systems. As discussed previously, our hypothesis is that the high permeability of the medium favors momentum transfers between the two phases. For $\frac{1}{\mathcal{N}_g} \sim 0.01$ (Re$_d \sim 30$), even the model with cross terms deviates from experimental results, an effect that is likely due to inertial effects [3,17] that start to become significant as the flow rate is increased.

We show in Fig. 5, using different colors, that the nature of the propagation front can change depending on $\mathcal{N}_g$. The propagation fronts of water S_w are presented for each of the different regimes in Fig. 6 in the presence and absence of cross terms. The construction of the shocks is outlined only for the model including cross terms. This is the front S_a (air phase) that is computed using the Buckley-Leverett theory, since we consider the injection of the air in the column (drainage). However, for consistency with other cases in the paper, we always consider the profile of the wetting phase in the transient regime (S_w here). Figures 6(a) and 6(b) correspond to a gravity-dominated regime (high gravity number $\frac{1}{\mathcal{N}_g} = 2 \times 10^{-3}$) where air propagates as a single front and where the impact of the cross terms is moderate. For lower values of $\mathcal{N}_g$ ($\frac{1}{\mathcal{N}_g} = 2 \times 10^{-2}$) [Figs. 6(c) and 6(d)], the model with cross terms yields a rarefaction wave. For $\frac{1}{\mathcal{N}_g} = 4 \times 10^{-2}$, in Figs. 6(e) and 6(f), the two models generate very different front profiles, with a single rarefaction wave for the model with cross terms. At steady state, however, this range of gravity numbers is not necessarily relevant as it corresponds to flow rates for which inertial effects are expected to be significant.

B. Imbibition: Air-water flow in highly permeable media

Here we proceed to the computation of the boundary-value problem presented in Fig. 2(b), with water injected within a medium initially saturated with air. The gas phase is initially at rest while water is injected at a constant flow rate and we vary the inlet flow rate from very low inlet velocities (high gravity number $\mathcal{N}_g$) to relatively high inlet velocities (low $\mathcal{N}_g$). We adopt the simplified annular viscous flow closures for the effective parameters (see Sec. II D 2).

We analyze the flow properties at steady state. Figure 7 shows the profiles of water saturation S_w and dimensionless pressure gradient $\frac{1}{\rho_a g} \frac{\partial P}{\partial x}$ as a function of the inverse of the gravity number, $\frac{1}{\mathcal{N}_g}$. As observed in the case of drainage, the generalized Darcy law without cross terms leads to a
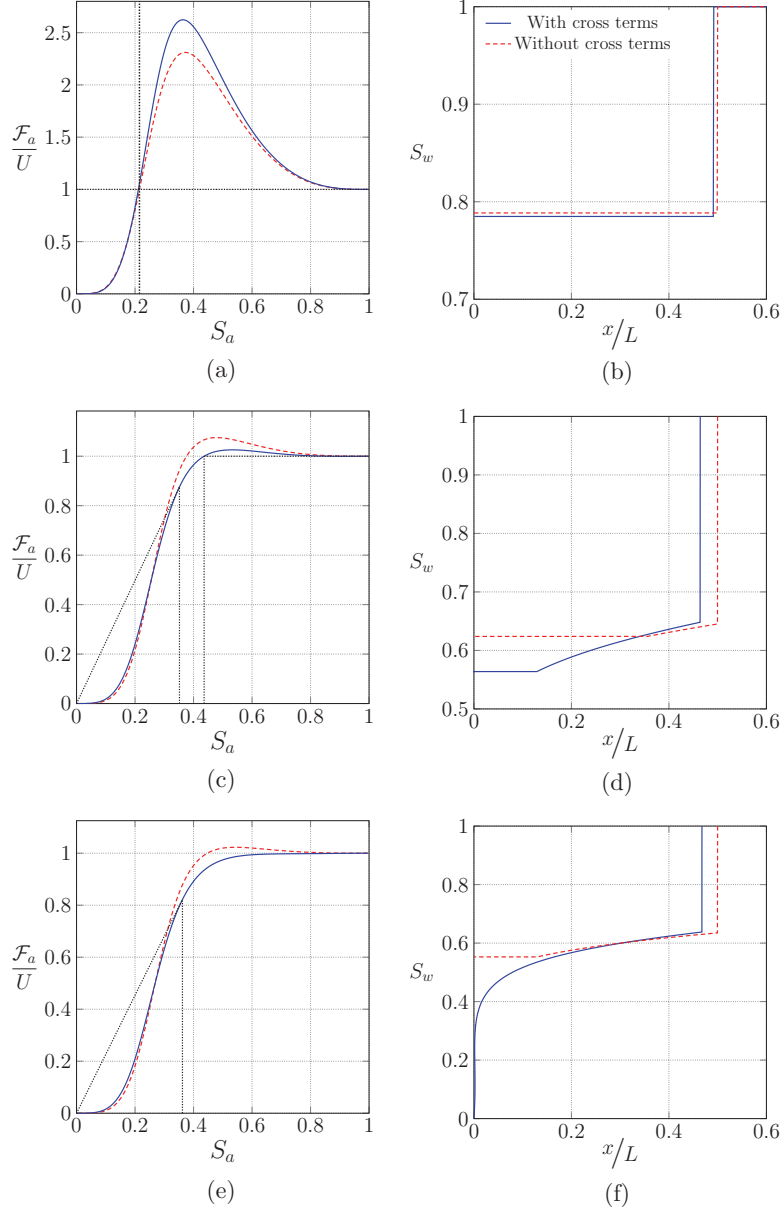
FIG. 6. Profiles of the water saturation S_w with (solid lines) and without (dashed lines) cross terms for different gravity numbers $\mathcal{N}_g$ (right) and the corresponding flux functions $\mathcal{F}_w$ nondimensionalized by the total velocity U (left): (a) and (b) $\frac{1}{\mathcal{N}_g} = 2 \times 10^{-3}$, (c) and (d) $\frac{1}{\mathcal{N}_g} = 2 \times 10^{-2}$, and (e) and (f) $\frac{1}{\mathcal{N}_g} = 4 \times 10^{-2}$. The profiles are given at the time corresponding to the front reaching half of the domain, i.e., $t = \frac{0.5L}{\hat{\mathcal{F}}_w'(S_w|_{\text{front}})}$, using the model without cross terms, with L the domain length and $\hat{\mathcal{F}}_w'(S_w|_{\text{front}})$ the water front speed [see Eq. (A4)].

pressure drop that is balanced by $\rho_a g$ regardless of the flow rate. The model with cross terms, on the other hand, generates significant variations of the pressure drop, from $\frac{\partial P}{\partial x} = \rho_a g$ at high $\mathcal{N}_g$ (low flow rates) to $\frac{\partial P}{\partial x} = \rho_w g$ at low $\mathcal{N}_g$ (high flow rates). Overall, the effect of the cross terms is also to *retain water* within the medium at moderate gravity number ($\frac{1}{\mathcal{N}_g} \gtrsim 0.5$), which corresponds to
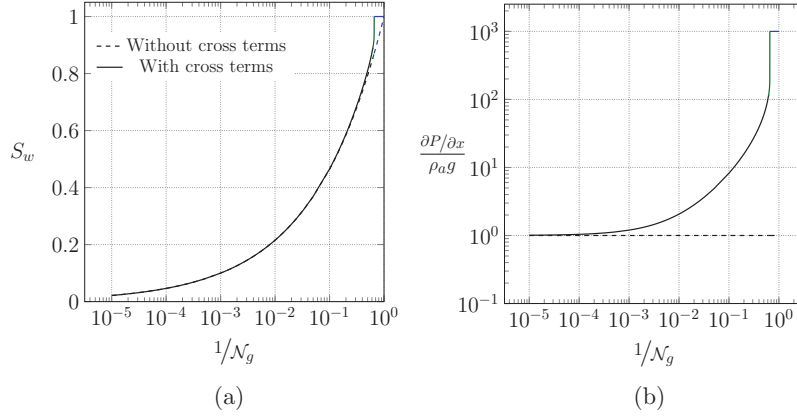
FIG. 7. Comparison of steady-state profiles with and without cross terms as a function of $\frac{1}{\mathcal{N}_g}$ with (a) water saturation and (b) the dimensionless pressure gradient. The colors distinguish different regimes of $\mathcal{N}_g$, with a shock (black), a rarefaction wave (blue), or both (green) (see also Fig. 8).

flow rates where water invades almost entirely the medium. For higher gravity numbers ($\frac{1}{\mathcal{N}_g} \lesssim 0.5$), the impact of the cross terms upon the saturation is limited, suggesting that cross terms are of little importance for large values of $\mathcal{N}_g$.

This result only applies to the one-dimensional Buckley-Leverett configuration with cocurrent flow presented here. There are other situations where cross terms may be important even in the limit of large values of $\mathcal{N}_g$. For instance, in structured packings used for separation processes, a thin liquid film is strongly sheared by a countercurrent gas phase and often displays surface instabilities. The fact that both phases flow countercurrently ($K_{wa}U_a \neq 0$) combined with the development of instabilities (larger values of K_{wa}) may greatly increase the impact of cross terms, potentially leading to strong liquid retention [57]. Our results then suggest that the quantitative analysis of the retention phenomenon requires an accurate estimation of the coupling terms, something often overlooked in the literature.

In Fig. 7 we see that the nature of the fronts in the dynamic regime can change depending on the intensity of the flow rate with different colors indicating different regimes. This is detailed in Fig. 8 in the presence and absence of cross terms for different values of $\mathcal{N}_g$. The water profile is plotted at a given time for each case, along with the corresponding flux functions $\mathcal{F}_w$ depending on the water saturation S_w. As before, the construction of the shocks is outlined only for the model including cross terms, along with a sketch of the characteristic curves in the x-t plane. Figure 8 shows that there is an increasing effect of the cross terms with $\frac{1}{\mathcal{N}_g}$, on both the dynamics and steady state. In Figs. 8(a) and 8(b) we see that for $\frac{1}{\mathcal{N}_g}$ small ($\frac{1}{\mathcal{N}_g} = 10^{-1}$), the regime is dominated by gravity and the water phase propagates as a single front. In this regime cross terms weakly impact the dynamics of the flow and the steady state (Fig. 7). For lower gravity numbers ($\frac{1}{\mathcal{N}_g} \gtrsim 0.5$), as plotted in Figs. 8(c)–8(h), the cross terms significantly impact the profiles of the fronts. The propagation of the saturation front is slowed down because of the transfer of momentum from water to the air. Further, the model with cross terms yields a rarefaction wave for $\frac{1}{\mathcal{N}_g} = 0.65$ and $\frac{1}{\mathcal{N}_g} = 0.83$ [Figs. 8(c) and 8(d) and Figs. 8(e) and 8(f), respectively], while the model without cross terms leads to a single front for a wider range of $\mathcal{N}_g$. Finally, in Figs. 8(g) and 8(h), which correspond to $\frac{1}{\mathcal{N}_g} = 1.1$, the model with cross terms yields a single shock that propagates through the entire medium, while the model without cross terms recovers the traditional Buckley-Leverett solution.
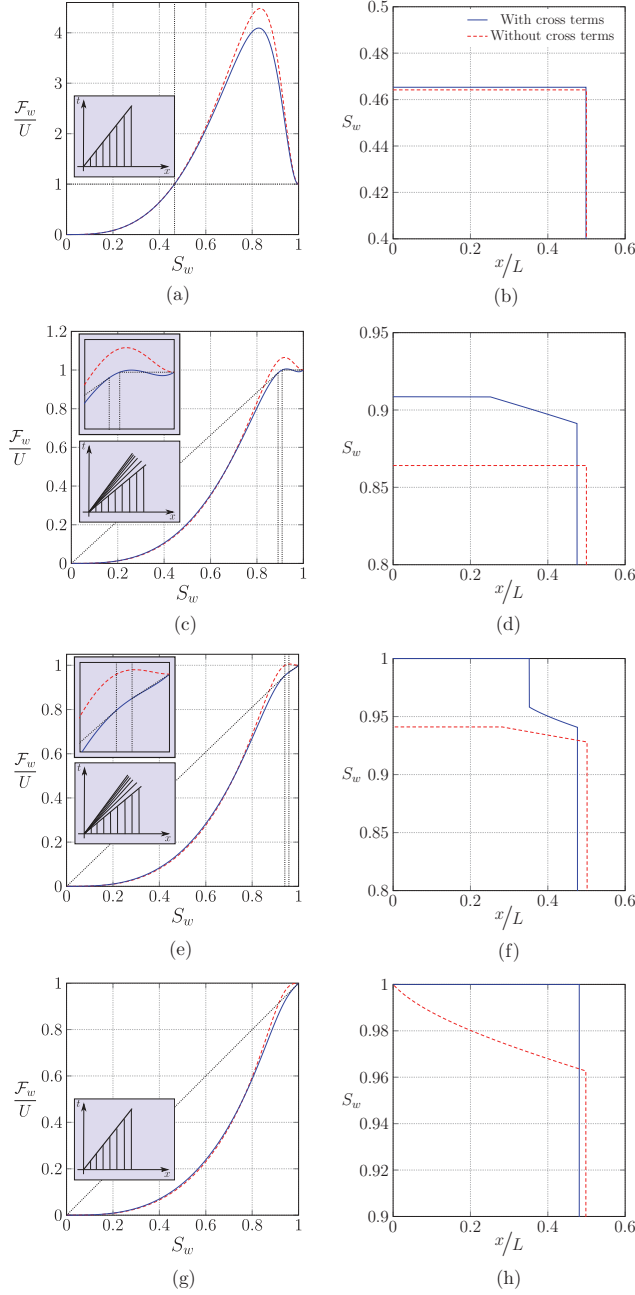
FIG. 8. Profiles of the water saturation S_w for different gravity numbers $\mathcal{N}_g$ (right) and the corresponding flux functions $\mathcal{F}_w$ nondimensionalized by the total velocity U (left): (a) and (b) $\frac{1}{\mathcal{N}_g} = 0.1$, (c) and (d) $\frac{1}{\mathcal{N}_g} = 0.65$, (e) and (f) $\frac{1}{\mathcal{N}_g} = 0.83$, and (g) and (h) $\frac{1}{\mathcal{N}_g} = 1.1$. The profiles are given at the time corresponding to the front reaching half of the domain, i.e., $t = \frac{0.5L}{\hat{\mathcal{F}}'_w(S_w|_{\text{front}})}$, using the model without cross terms, with L the domain length and $\hat{\mathcal{F}}'_w(S_w|_{\text{front}})$ the water front speed [see Eq. (A4)]. The dashed lines correspond to the model without cross terms and the solid lines to the model with cross terms. Insets highlight the construction of the shocks for the case with cross terms, with indications on the position of the shocks and plots of the characteristic curves in the x-t plane.
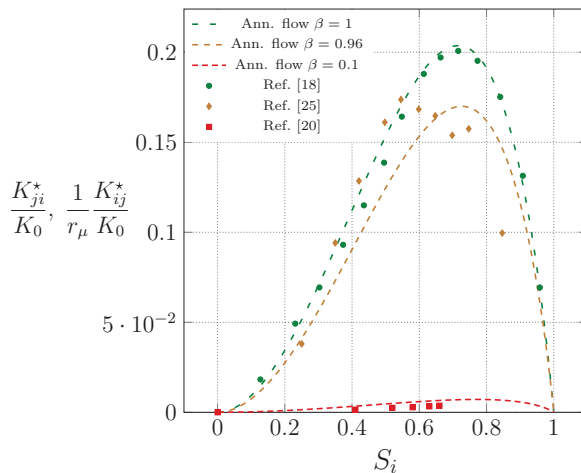
FIG. 9. Comparison of nondimensionalized cross terms for multiple weighting factors β [dashed lines; see Eq. (24)] to experimental results from [18,20] and numerical results from [25]. Here $\frac{K_{ij}^{\star}}{K_0}$ and $\frac{K_{ji}^{\star}}{K_0 r_\mu}$ are plotted as functions of the saturation S_i.

C. Imbibition: Oil-water flow in low-permeability media

We now consider the constant injection of water in a porous medium of low permeability initially saturated with oil, which is a case of importance in petroleum engineering. As discussed in the Introduction, we expect the fluid-solid interface to play a much important role in this case, especially when fluid phases flow in distinct pore networks and momentum exchange between the two fluid phases is negligible. Can we include this effect in the formulation with the cross-term coefficients K_{wo} and K_{ow}?

In order to do so, we hypothesize that the separation into different flow paths and the relative influence of fluids-solid and fluid-fluid interfaces can be represented by a scalar coefficient $\beta \in [0,1]$, weighting the cross terms

$$K_{wo}(\beta) = \beta K_{wo}, \quad K_{ow}(\beta) = \beta K_{ow}. \tag{24}$$

Here $K_{wo}(\beta)$ and $K_{ow}(\beta)$ are cross terms from the annular viscous closures that are simply weighted by β. As before, the K coefficients are based on the analytical solution of the annular two-phase flow (21). However, we do not use the simplified expressions ($\frac{\mu_j}{\mu_i} \ll 1$), since $\frac{\mu_o}{\mu_w} = 100$ in the case of oil and water.

We compare in Fig. 9 the profiles of $\frac{K_{ji}^{\star}}{K_0} = \frac{1}{r_\mu} \frac{K_{ij}^{\star}}{K_0}$ as functions of S_i for different values of β to experimental measurements from [18,20]. Kalaydjian showed experimentally and analytically, using multiple couples of fluids, that the maximum value of the dimensionless cross terms $\frac{K_{ji}^{\star}}{K_0} = \frac{1}{r_\mu} \frac{K_{ij}^{\star}}{K_0}$ obtained for capillary tubes with a square section is ~ 0.2. Zarcone and Lenormand [20] performed measurements of the cross terms for mercury and water flows in a sand pack. They found that the magnitude of the cross terms is much less important in their case than in experiments using capillary tubes with a square section. They measured that the dimensionless cross terms are at most $\sim 4 \times 10^{-3}$, which is well below ~ 0.2. As discussed in the Introduction, their primary hypothesis is that this weaker influence stems from the smaller interfacial area between the two phases.

These experimental results are plotted in Fig. 9, along with our weighted representation of the coupling terms. Importantly, we see that changing the value of β allows us to recover both results for the sand and capillaries. For the sand we have $\beta \sim 0.1$, which confirms that the momentum exchange is smaller in low-permeability media than in capillaries. Numerical results from Rothman in [25], consisting of two-phase flow calculations in a pore network of large permeability, are also
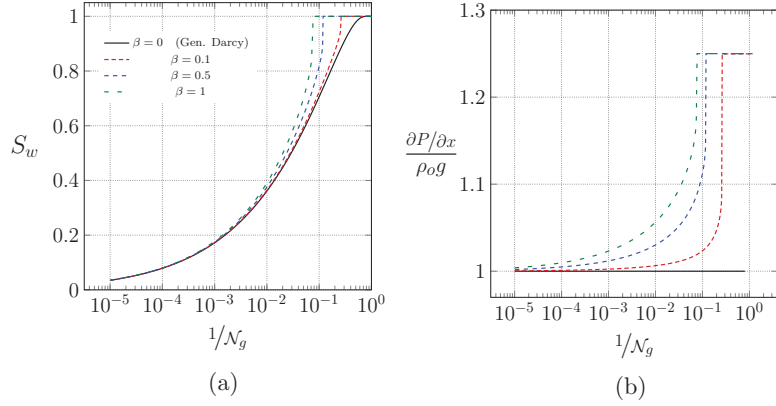
-

FIG. 10. Comparison of steady-state profiles for different values of the coefficient β with (a) water saturation and (b) the dimensionless pressure gradient at steady state as a function of $\frac{1}{\mathcal{N}_g}$.

plotted for comparison. This case is intermediate between the sand pack and the capillaries, with a maximum value of the cross terms, ~ 0.17, that is slightly below the one obtained for capillaries. These results are captured by using a weighting value $\beta \sim 0.96$. We conclude that only one scalar coefficient captures the trend of the coupling coefficients for different media. However, a great deal of work remains to be done to derive proper constitutive relations for each effective parameter and each case. This means that a better understanding of the link between the pore-scale physics and the macroscale behavior is needed, maybe through pore-scale simulations of the two-phase flows and new experimental designs.

Based on these observations, we simulate the injection of water in a low-permeability medium ($K_0 = 10^{-11}$ m^2) initially filled with oil. The influence of the cross terms on the flow properties (multiple values of β) is presented in Fig. 10 at steady state as a function of the gravity number. The pressure drop and the quantity of oil that is recovered are highly affected by the value of β, especially for moderate values of $\mathcal{N}_g$ ($\frac{1}{\mathcal{N}_g} \gtrsim 0.01$). This is confirmed in the dynamic regime for $\frac{1}{\mathcal{N}_g} = 0.1$, in Fig. 11, where the profiles are considerably modified by the value of β. For $\beta \ll 1$, the profile consists in a single gravity shock with a moderate displacement of the oil, whereas
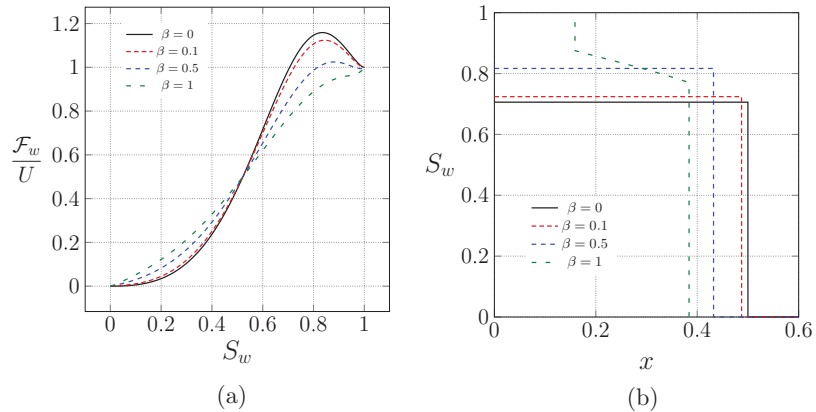

FIG. 11. Comparison of dynamic profiles for different values of the coefficient β with (a) the flux functions $\mathcal{F}_w$ nondimensionalized with the total velocity U at $\frac{1}{\mathcal{N}}=0.1$ and (b) the corresponding profiles of water saturation S_w at a given time.

for $\beta = 1$, water displaces the oil phase entirely. This result for $\beta = 1$ is unrealistic and seems to indicate that the capillary tube solution overestimates the coupling effects in low-permeability media. This is also consistent with the experimental results from Zarcone and Lenormand, whose measurements correspond to $\beta \sim 0.1$. We therefore hypothesize that the permeability of the porous structure is key in evaluating the impact of the cross terms, as it controls the relative influence of the fluid-solid and fluid-fluid interfaces. For low-permeability media, the fluid-solid interface may dominate momentum transport, possibly due to a separation of flow paths for the two fluids, which may limit momentum exchanges. In contrast, highly permeable media may yield a relatively smaller influence of the fluid-solid interface and favor film, bubble, or annular flows that generate more exchanges.

IV. CONCLUSION

In this paper we studied the influence of momentum coupling effects for two-phase creeping flows of immiscible fluids in porous media. Our analysis is based on the Buckley-Leverett theory in a one-dimensional setting, which is extended to account for cross terms in the models. We considered two boundary-value problems corresponding to two classical configurations encountered in porous media applications (drainage and imbibition). We studied different couples of fluids and different closure relations for the effective parameters and compared our results to experimental data.

Our main result is that the cross terms can significantly affect the flux functions, the dynamics of saturation fronts, and the steady states, in ways that are confirmed experimentally and therefore physically realistic. This is important because these cross terms are generally assumed to be negligible in the momentum balance. Our hypothesis is that, for the low-permeability media considered in many studies, the fluid-solid interface dominates momentum transport, therefore limiting the influence of fluid-fluid exchanges. Depending on the wettability, capillary action, and pore-size distribution, low-permeability media also favor the appearance of preferential flow paths for the phases and therefore further limit momentum exchange by reducing the fluid-fluid interfacial area. In contrast, highly permeable media may yield large fluid-fluid interfaces relative to the fluid-solid ones, therefore maximizing exchanges. This is particularly obvious when comparing the experimental results from the literature to our theoretical results.

To get one step further in the description of such systems, we need experiments that measure simultaneously the flow at the pore scale and the macroscale for a broad range of permeabilities. Further, we need to go beyond the creeping flow limit that proved to be limiting in describing experiments from [3]. Similar models, including additional drag terms accounting for inertial effects, can be used for this purpose [35]. The analysis of such models may be of importance in many applications involving flows at high Reynolds numbers, for instance, in chemical exchangers or debris beds.

APPENDIX: UNIQUE SOLUTION OF THE CONSERVATION LAW

The solution $S_i(x,t)$ of the two-phase system is determined by considering the Riemann problem that is associated with Eqs. (15). It reads

$$\varepsilon \frac{\partial S_i}{\partial t} + \frac{\partial \mathcal{F}_i}{\partial x} = 0, \tag{A1a}$$

$$S_L = S_i(0,t), \tag{A1b}$$

$$S_R = S_i(x,0), \tag{A1c}$$

with $S_L > S_R$.

The inlet value S_L is not known *a priori*, but verifies the equation of the inlet flow rate $\mathcal{F}_i(S_L) = U(0,t) = U_i(0,t)$ [Eq. (15c)]. Given the conditions presented in Sec. II A 2, $S_L = 1$ is always a

solution of this equation, but other values can also be solutions when gravity effects dominate over viscous effects ($\mathcal{N}_g > 1$) [52].

The unique admissible solution of the system (A1) is determined by constructing the concave hull [51,52] $\hat{\mathcal{F}}_i$, which is defined on the interval $[S_R, S_L]$ as

$$\hat{\mathcal{F}}_i = \inf_{h \in \mathcal{C}}(h), \tag{A2}$$

with $\mathcal{C}$ the ensemble of concave functions such that $h \in \mathcal{C}$ is equivalent to

$$h(S_i) > \mathcal{F}_i(S_i), \quad \forall S_i \in [S_R, S_L]. \tag{A3}$$

By construction, we obtain a number of intermediate points $\{S_k\}_0^{n+1}$ such that $S_R < S_1 < S_k < S_n < S_L$, with $k \in [0,n]$ and where the $n + 1$ points correspond to the intersection points between $\hat{\mathcal{F}}_i$ and $\mathcal{F}_i$ [52]. On each of the intervals $[S_k, S_{k+1}]$, $\hat{\mathcal{F}}_i$ either coincides with $\mathcal{F}_i$ or connects linearly $\hat{\mathcal{F}}_i(S_k)$ to $\hat{\mathcal{F}}_i(S_{k+1})$. In the former case, the solution between S_k and S_{k+1} consists in a rarefaction wave, while in the second case the solution is a shock that propagates with the speed

$$\hat{\mathcal{F}}_i'(S_{k+1}) = \frac{\mathcal{F}_i(S_{k+1}) - \mathcal{F}_i(S_k)}{S_{k+1} - S_k}, \quad k \in [0,n]. \tag{A4}$$

This relation is the Rankine-Hugoniot condition. The solution must also verify the Oleinik entropy constraint, which reads

$$\frac{\mathcal{F}_i(S_i) - \mathcal{F}_i(S_{k+1})}{S_i - S_{k+1}} \geqslant \hat{\mathcal{F}}_i'(S_{k+1}) \geqslant \frac{\mathcal{F}_i(S_i) - \mathcal{F}_i(S_k)}{S_i - S_k}, \quad \forall S \in [S_k, S_{k+1}]. \tag{A5}$$

The characteristic curves of the system in the x-t plane verify

$$\frac{dx}{dt} = \hat{\mathcal{F}}_i'(S_i), \quad \forall S_i \in [S_R, S_L], \tag{A6}$$

leading to equations for the characteristic curves [see Fig. 1(c)]

$$x = \hat{\mathcal{F}}_i'(S_i)t + r, \quad \forall S_i \in [S_R, S_L], \tag{A7}$$

where r parametrizes the position of x at $t = 0$.

If the inlet condition (15c) admits more than one solution [as illustrated in Figs. 1(d)–1(f)], which is encountered when gravity effects dominate viscous effects, we select the minimum of the solutions of Eq. (15c), $\mathcal{F}_i(S_i) = U(0,t) = U_i(0,t)$, which corresponds to a positive shock speed. In the case illustrated in Fig. 1(e), this corresponds to a unique shock between S_L and S_R given by the Rankine-Hugoniot condition

$$\hat{\mathcal{F}}_i'(S_L) = \frac{\mathcal{F}_i(S_L) - \mathcal{F}_i(S_R)}{S_L - S_R}. \tag{A8}$$

[1] J. Bear, *Dynamics of Fluids in Porous Media* (Elsevier, New York, 1972).

[2] L. W. Lake, *Enhanced Oil Recovery* (Prentice Hall, Englewood Cliffs, 1989).

[3] N. Chikhi, R. Clavier, J.-P. Laurent, F. Fichot, and M. Quintard, Pressure drop and average void fraction measurements for two-phase flow through highly permeable porous media, Ann. Nucl. Energy **94**, 422 (2016).

[4] F. Fichot, F. Duval, N. Trégourès, C. Béchaud, and M. Quintard, The impact of thermal non-equilibrium and large-scale 2D/3D effects on debris bed reflooding and coolability, Nucl. Eng. Des. **236**, 2144 (2006).

[5] M. Muskat, *The Flow of Homogeneous Fluids through Porous Media* (Mapple, York, 1946).

[6] M. Honarpour, L. Koederitz, and A. H. Harvey, *Relative Permeability of Petroleum Reservoirs* (CRC, Boca Raton, 1986).

[7] J.-L. Auriault, Nonsaturated deformable porous media: Quasistatics, Transp. Porous Media **2**, 45 (1987).

[8] L. Cueto-Felgueroso and R. Juanes, A phase field model of unsaturated flow, Water Resour. Res. **45**, W10409 (2009).

[9] W. G. Gray and S. M. Hassanizadeh, Macroscale continuum mechanics for multiphase porous-media flow including phases, interfaces, common lines and common points, Adv. Water Resour. **21**, 261 (1998).

[10] M. Hassanizadeh and W. G. Gray, Toward an improved description of the physics of two-phase flow, Adv. Water Resour. **16**, 53 (1993).

[11] R. Hilfer, Macroscopic equations of motion for two-phase flow in porous media, Phys. Rev. E **58**, 2090 (1998).

[12] F. Kalaydjian, A macroscopic description of multiphase flow in porous media involving spacetime evolution of fluid/fluid interface, Transp. Porous Media **2**, 537 (1987).

[13] M. Panfilov and I. Panfilova, Phenomenological meniscus model for two-phase flows in porous media, Transp. Porous Media **58**, 87 (2005).

[14] M. Quintard and S. Whitaker, Two-phase flow in heterogeneous porous media I: The influence of large spatial and temporal gradients, Transp. Porous Media **5**, 341 (1990).

[15] P. C. Reeves and M. A. Celia, A functional relationship between capillary pressure, saturation, and interfacial area as revealed by a pore-scale network model, Water Resour. Res. **32**, 2345 (1996).

[16] S. Whitaker, Flow in porous media: The governing equations for immiscible, two-phase flow, Transp. Porous Media **1**, 105 (1986).

[17] R. Clavier, N. Chikhi, F. Fichot, and M. Quintard, Modeling of inertial multi-phase flows through high permeability porous media: Friction closure laws, Int. J. Multiphase Flow **91**, 243 (2017).

[18] F. Kalaydjian, Origin and quantification of coupling between relative permeabilities for two-phase flows in porous media, Transp. Porous Media **5**, 215 (1990).

[19] W. Rose, Coupling coefficients for two-phase flow in pore spaces of simple geometry, Transp. Porous Media **5**, 97 (1990).

[20] C. Zarcone and R. Lenormand, Détermination expérimentale du couplage visqueux dans les écoulements diphasiques en milieu poreux, Soil Mech. Porous Media **318**, 1429 (1994).

[21] R. G. Bentsen and A. A. Manai, On the use of conventional cocurrent and countercurrent effective permeabilities to estimate the four generalized permeability coefficients which arise in coupled, two-phase flow, Transp. Porous Media **11**, 243 (1993).

[22] B. J. Bourbiaux and F. J. Kalaydjian, Experimental study of cocurrent and countercurrent flows in natural porous media, SPE Reservoir Eng. **5**, 361 (1990).

[23] W. Rose, Measuring transport coefficients necessary for the description of coupled two-phase flow of immiscible fluids in porous media, Transp. Porous Media **3**, 163 (1988).

[24] M. Danis and M. Quintard, Modélisation d'un écoulement diphasique dans une succession de pores, Rev. Institut Français Pétrole **39**, 37 (1984).

[25] D. H. Rothman, Macroscopic laws for immiscible two-phase flow in porous media: Results from numerical experiments, J. Geophys. Res.: Solid Earth **95**, 8663 (1990).

[26] I. Iliuta, M. Fourar, and F. Larachi, Hydrodynamic model for horizontal two-phase flow through porous media, Can. J. Chem. Eng. **81**, 957 (2003).

[27] R. J. Lipinski, Model for boiling and dryout in particle beds, Sandia National Laboratories Report No. SAND82-0765, 1982 (unpublished).

[28] T. Schulenberg and U. Müller, An improved model for two-phase flow through beds of coarse particles, Int. J. Multiphase Flow **13**, 87 (1987).

[29] N. K. Tutu, T. Ginsberg, T. Klein, J. Klages, and C. Schwarz, Debris bed quenching under bottom flood conditions (in-vessel degraded core cooling phenomenology), Brookhaven National Laboratories Report No. NUREG/CR-3850, 1986 (unpublished).

[30] V. X. Tung and V. K. Dhir, On fluidization of a particulate bed during quenching by flooding from the bottom, University of California, Los Angeles Report No. EPRI-NP–4455, 1986 (unpublished).

[31] P. A. C. Raats, Applications of the theory of mixtures in soil science, Math. Model. **9**, 849 (1987).

[32] G. Baveye and P. Sposito, The operational significance of the continuum hypothesis in the theory of water movement through soils and aquifers, Water Resour. Res. **20**, 521 (1984).

[33] M. Hassanizadeh and W. G. Gray, General conservation equations for multi-phase systems: 3. Constitutive theory for porous media flow, Adv. Water Resour. **3**, 25 (1980).

[34] C. M. Marle, On macroscopic equations governing multiphase flow with diffusion and chemical reactions in porous media, Int. J. Eng. Sci. **20**, 643 (1982).

[35] D. Lasseux, A. Ahmadi, and A. Arani, Two-phase inertial flow in homogeneous porous media: A theoretical derivation of a macroscopic model, Transp. Porous Media **75**, 371 (2008).

[36] S. R. Shadizadeh and A. Hashemi, The impact of reservoir properties on pseudo functions: Upscaling of relative permeability, Petrol. Sci. Technol. **32**, 772 (2005).

[37] J. W. Barker and S. Thibeau, A critical review of the use of pseudorelative permeabilities for upscaling, SPE Reserv. Eng. **12**, 138 (1997).

[38] C. Soulaine, P. Horgue, J. Franc, and M. Quintard, Gas-liquid flow modeling in columns equipped with structured packing, AIChE J. **60**, 3665 (2014).

[39] M. Quintard and S. Whitaker, Two-phase flow in heterogeneous porous media: The method of large-scale averaging, Transp. Porous Media **3**, 357 (1988).

[40] D. Lasseux, M. Quintard, and S. Whitaker, Determination of permeability tensors for two-phase flow in homogeneous porous media: Theory, Transp. Porous Media **24**, 107 (1996).

[41] S. E. Buckley and M. C. Leverett, Mechanism of fluid displacement in sands, Soc. Petrol. Eng. **146**, 107 (1942).

[42] P. Bedrikovetsky, *Mathematical Theory of Oil and Gas Recovery* (Springer, Berlin, 1993).

[43] C. Cancès, Finite volume scheme for two-phase flows in heterogeneous porous media involving capillary pressure discontinuities, ESAIM: Math. Model. Numer. Anal. **43**, 973 (2009).

[44] F. Doster and R. Hilfer, Generalized Buckley-Leverett theory for two-phase flow in porous media, New J. Phys. **13**, 123030 (2011).

[45] J. Hagoort, Oil recovery by gravity drainage, Soc. Petrol. Eng. J. **20**, 139 (1980).

[46] E. F. Kaasschieter, Solving the Buckley-Leverett equation with gravity in a heterogeneous porous medium, Comput. Geosci. **3**, 23 (1999).

[47] A. Ahmadi, A. Arani, and D. Lasseux, Numerical simulation of two-phase inertial flow in heterogeneous porous media, Transp. Porous Media **84**, 177 (2010).

[48] P. Horgue, C. Soulaine, J. Franc, R. Guibert, and G. Debenest, An open-source toolbox for multiphase flow in porous media, Comput. Phys. Commun. **187**, 217 (2015).

[49] P. D. Lax, *Hyperbolic Systems of Conservation Laws and the Mathematical Theory of Shock Waves* (Society for Industrial and Applied Mathematics, Philadelphia, 1973).

[50] E. F. Toro, *Riemann Solvers and Numerical Methods for Fluid Dynamics: A Practical Introduction* (Springer, Berlin, 1997).

[51] S. Diehl, On scalar conservation laws with point source and discontinuous flux function, J. Math. Anal. **26**, 1425 (1993).

[52] W. Proskurowski, A note on solving the Buckley-Leverett equation in the presence of gravity, J. Comput. Phys. **41**, 136 (1981).

[53] A. Riaz and H. Tchelepi, Stability of two-phase vertical flow in homogeneous porous media, Phys. Fluids **19**, 072103 (2007).

[54] R. Clavier, Étude expérimentale et modélisation des pertes de pression lors du renoyage d'un lit de débris, Ph.D. thesis, Institut National Polytechnique de Toulouse, 2015, available at http://oatao.univ-toulouse.fr/14705/

[55] P. Horgue, Modélisation multi-échelle d'un écoulement gaz-liquide dans un lit fixe de particules, Ph.D. thesis, Institut de Mécanique des Fluides de Toulouse, 2012, available at http://oatao.univ-toulouse.fr/6991/

[56] R. H. Brooks and A. T. Corey, Hydraulic properties of porous media, Hydrology Papers 3, Colorado State University, 1964 (unpublished).

[57] P. Suess and L. Spiegel, Hold-up of Mellapak structured packings, Chem. Eng. Process. **31**, 119 (1992).